Structural Topology Optimization of Reactionless Four-bar Linkages

Juan Emmanuel Ayala Hernandez, Sébastien Briot, Jesus Cervantes-Sanchez

Structural Topology Optimization of Reactionless Four-bar Linkages

J. Emmanuel Ayala-Hernández[a,b,c] **Sébastien Briot**[c,d*]

J. Jesús Cervantes-Sánchez[a]

[a]University of Guanajuato
Department of Mechanical Engineering, DICIS
Salamanca 36885, Guanajuato, México

[b]École Centrale de Nantes
1 rue de la noë 44321 Nantes, France

[c]Laboratoire des Sciences du Numérique de Nantes (LS2N)
1 rue de la noë 44321 Nantes, France

[d]Centre National de la Recherche Scientifique (CNRS)

Emails: {Emmanuel.Ayala, Sebastien.Briot}@ls2n.fr, jecer@ugto.mx

Classical dynamic balancing techniques do not consider the linkage elastic behavior. For mechanism or robot design purpose, taking into account the flexibility of the multibody system is of the utmost importance, in order to be able to manufacture a mechanism / robot which is stiff enough for a given task. This paper deals with a novel approach that allows to design mechanisms by means of structural topology optimization while specific dynamic balancing conditions are considered. In our work, the links are treated as three-dimensional flexible bodies, and the optimization process is performed for all the bodies simultaneously. Applying this methodology, the optimal design of a dynamically balanced four-bar linkage is accomplished while its compliance is minimized.

Numerical validations of the optimized linkage properties are carried out using commercial software. The dynamic balancing performance of the optimized four-bar linkage is numerically validated using ADAMS. Besides, ANSYS software was used in order to perform the linkage stiffness analysis and to compare it with the results of the optimization solver.

In order to verify the feasibility of the proposed methodology, a prototype is built. Experimental studies are carried out in order to evaluate its dynamic balancing performance.

1 INTRODUCTION

During high-speed tasks, large accelerations of mechanisms and robots lead to the generation of high inertial forces and moments, which are transmitted to the ground, causing the so-called shaking forces and shaking moments. These fluctuating loads are a significant source of vibration excitation, and lead to noise, fatigue and wear [1]. However, they can be canceled or reduced by suitable dynamic balancing techniques. Thus, if a mechanism does not exert any unbalanced reaction at its base it is called a "reactionless" or a "dynamically balanced" mechanism.

Shaking forces and moments can be reduced or eliminated using specific mechanism design, and proper inertia parameters. In order to obtain a reactionless mech-

*Corresponding author.

anism, classical techniques like the addition of counterweights [2, 3], counter-rotations [4, 5, 6, 7], or also auxiliary mechanisms [8, 9, 10, 11] can be deployed. Other researchers have proposed alternatives, like dynamic balancing via optimal motions of robot moving links [12, 13, 14, 15, 16], or the design of reactionless robots based on the dynamically balanced four-bar linkage (deleting the counter-rotations) [17, 18, 19]. Besides, another approach for dynamic balancing is the so-called inherent balancing method, which uses all elements of the mechanism to contribute to the motion and the dynamic balance [20, 21]. Exhaustive reviews of the classical balancing techniques can be found in [22, 23].

In general, the solution of the classical dynamic balancing methods have the following major drawback: the total mass / inertia in the system is increased. In order to decrease the system mass or inertia, a temptation could be to lighten the initial mechanism, at the price of a decrease of its stiffness performances, making the mechanism potentially no more viable for some given tasks. A better idea would be to optimize the design so that in parallel we may respect (or optimize) both balancing constraints and elastic performances (e.g. deformations, natural frequencies) in the same time in order to ensure that the manufactured balanced mechanism or robot is stiff enough for a given task. Indeed, finding a way to optimize the design of a dynamically balanced mechanism or robot under elastic behavior constraints or objectives is a very complicated task, but it is an important issue to be solved in high-speed robot design, which is the aim of the present work.

In order to avoid the addition of counter-rotations, the works [18, 19] proposed to design parallel robots by using some particular reactionless four-bar linkages [17]. Indeed, it was shown in [17] that four-bar linkages can be fully balanced without the addition of counter-rotations or any auxiliary linkages by forcing a combination of geometric relationships and proper mass distributions. Therefore, it is possible to exploit these self-balanced four-bar linkages as special modules for building reactionless robots.

For robot design purposes, obtaining reactionless four-bar linkage is of interest, but is usually necessary to optimize other performances in parallel. There are some works which explored the external link shape optimization in order to minimize the inertial forces and moments. Thus, in [24] the authors performed dynamic optimization of the planar four-bar linkage controlling the changes in the joint forces while the joint clearances are considered. In addition a technique called "small element superposing method" was proposed in order to generate the external link shape, based on the optimized link parameters. This technique does not take into account the elasticity of the links in its formulation. Another optimization framework approach to optimize the four-bar linkage was proposed in [25], where the authors used shape optimization based on the rigid body dynamics for optimizing the external link shape (only). Since the approach is based on rigid body formulation, the deformations of the link cannot be considered in the optimization, which is a problem because the mass and inertia reduction may lead to low stiffness link designs. Moreover, there is no possibility to modify the internal link shape (including some voids, for instance).

In all the aforementioned works, the linkage elastic performances (e.g. deformations under given loads, natural frequencies) are never optimized, while for robot design purposes, these performances are of the utmost importance. Therefore, in order to optimize the self-balanced four-bar linkage, and to take into account the elastic behavior of the links, in this research work we propose to use structural topology optimization (TO) [26] as a tool for the design of a reactionless four-bar linkage in order to optimize the mechanism stiffness while ensuring that the balancing constraints are respected. Structural topology optimization is a powerful mathematical method which aims to redistribute the material into an initial domain taking into account design specifications [26]. The optimization process is based on the structural response, typically computed by the finite element method (FEM). Therefore, using this approach, we address the optimal design of reactionless four-bar linkage as a flexible mechanical multibody system.

To the best of our knowledge, a single work attempts to solve the dynamic balancing of flexible multibody systems. The optimal design based on TO for a reactionless four-bar linkage was reported in [27]. In this work, the bodies were treated as planar ones, the first natural frequency was maximized, and the mechanism compliance was constrained while ensuring the balancing conditions. The results obtained in that work proved the potential of topology optimization as a valuable tool for linkage design under dynamic balancing constraints. Nevertheless, the optimized properties were not validated, and the links of four-bar linkage were considered as a planar bodies. This avoid the possibility to consider the links bending out of the plane motions, and restricts the optimal design for a planar loads system.

The design approach reported in the present paper introduces several advantages with respect to previously published researches related to dynamic balancing of flexible multibody systems, mainly with respect to [27]. At first, the links are treated as 3D flexible bodies, being thus possible to optimize the links for a general loading sys-

tem. Secondly, in order to validate the reliability of our solution proposal, numerical validations of the optimized properties were realized using specialized software. In third place, a prototype was built in order to carry out an experimental evaluation of the linkage dynamic balancing behavior. In our case study, we optimize the stiffness of the four-bar linkage by minimizing its compliance while the dynamic balancing conditions are satisfied. Optimizing the linkage stiffness can enhance the balancing performance since it prevent negative effects due to excessive deformations, such as wear, low accuracy, and even vibrations.

The paper is written as follows. Section 2 describes the modeling of the four-bar linkage as a flexible multibody system, and its dynamic balancing conditions. After that, Section 3 introduces the definition of the optimization problem; four different case studies are defined. Then, in Section 4, the results of the optimization process are analyzed, and we report the numerical validation of the optimized properties. In addition, in this section an experimental validation for the dynamic balancing is carried out. Finally, in Section 5, the conclusions of this research work are exposed.

2 PROBLEM FORMULATION

In the present paper, we perform the structural topology optimization of a reactionless four-bar linkage. Topology optimization uses FEM to model the body elastic behavior. The optimization problem of any multibody system involves the complete finite element model of n bodies connected by kinematic joints under boundary conditions [28, 29]. This generates a large model which requires an efficient problem formulation and suitable computational tools in order to find a solution in a reasonable amount of time [30].

The approach used in this paper is adapted from [30], where the authors addressed the topology optimization problem of multibody mechanical robotized systems, but where the balancing of the mechanism was not considered at all. The proposed methodology uses finite element formalism to model each body of the linkage, and these bodies are connected by ideal rigid joints. Additionally, model reduction techniques are applied in order to reduce the computational cost of solving the multibody model.

2.1 Elastostatic model of a single body

Usually the topology optimization problem [31, 32, 33, 34, 35, 36] is formulated for a single body, but in our case it is necessary to model a system composed for multiple bodies connected by kinematic joints. In order to describe the multibody system, we use subscripts to identify the element and the body. Thus the element j of the body i is defined by the subscript ij. Figure 1 is used to represent a general body $\mathcal{B}_i$, from where we can notice that the body has its own reference frame $O_i x_i y_i z_i$, and it is discretized in a regular mesh with N_i elements.

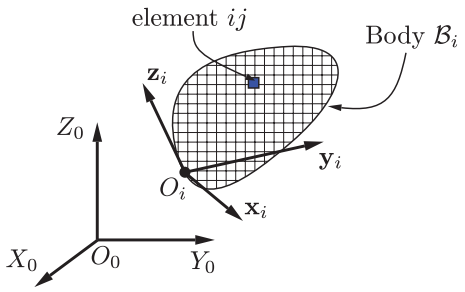

Fig. 1: General scheme of the body $\mathcal{B}_i$

Density-based topology optimization relies on the finite element method, and it uses finite elements of regular shape, where each element is associated with an artificial density, which is the design variable. The design variable is bound to take values between 0 and 1, however in order to avoid optimization results with several intermediate material densities, it is necessary to use a material interpolation scheme [26]. In this case, we use the modified simplified isotropic material with penalization (SIMP) interpolation scheme [37]. This method consists in assigning to each finite element a density ρ_{ij} that determines its Young's modulus E_{ij}. Therefore the modulus of elasticity for element j belonging to body $\mathcal{B}_i$ is given by:

$$E_{ij} = E_{\min} + \rho_{ij}^{p} \left(E_0 - E_{\min}\right), \text{ with } \rho_{ij} \in [0,\, 1]. \quad (1)$$

where p is the penalization power (usually $p = 3$, for elasticity problems), $E_{\min}$ is the stiffness at $\rho_{ij} = 0$ ($E_{\min}$ is different from 0 in order to avoid singularity of the stiffness matrix), and E_0 is the Young's modulus of the material.

By using finite element discretization, and resorting to the theory of linear elasticity, the stiffness matrix $K_{ij}(\rho_{ij})$ of a single element is written under the SIMP scheme as follows:

$$K_{ij} = E_{ij} K_{ij}^{(0)} = \left(E_{\min} + \rho_{ij}^{p} \left(E_0 - E_{\min}\right)\right) \mathbf{K}_{ij}^{(0)} \quad (2)$$

where $K_{ij}^{(0)}$ is a constant stiffness matrix for an element with Young's modulus equal to one.

Therefore, using the SIMP approach and based on the finite element formulation, the potential elastic energy of

the body $\mathcal{B}_i$ is computed as follows:

$$U_{e_i} = \frac{1}{2}\mathbf{u}_i^T \mathbf{K}_i \mathbf{u}_i \tag{3}$$

where matrix K_i is the body stiffness matrix, and u_i is the vector of independent coordinates. Thus, K_i is a stiffness matrix which relates the nodal displacements u_i to the forces f_i exerted on the nodes by the relation [29]:

$$\mathbf{f}_i = \frac{\partial U_{e_i}}{\partial \mathbf{u}_i} = \mathbf{K}_i \mathbf{u}_i \tag{4}$$

Equation (4) shows an explicit relation between the external loads acting in a single body and its nodal displacements. Normally, the nodal displacements are the variables to be computed, and the accuracy of the displacements relies upon body discretization. Nonetheless, the size of the stiffness matrix $\mathbf{K}_i$ depends on the number of elements in which the body is discretized: the larger the size, the longer the computation time. Thereby it is important to define the best trade-off between the mesh resolution and the computational cost.

The complete elastostatic model of the linkage can be derived using the body stiffness model given in Eq. (4). Nevertheless, if the formulation is used in this basic form, it generates a very large linkage stiffness matrix (in our case studies the dimension of K_i is typically greater than $10^5 \times 10^5$). Therefore, the use of a classical approach is not adequate for efficient computations, and it is necessary to apply a model reduction technique.

Using a model reduction technique, such as static condensation, it is possible to reduce the computational cost of solving the elastostatic model [38]. The reduction technique uses interface nodes: they are artificial nodes which control the surrounding nodes, in our case by a rigid connection. Basically, the rigid connection implies that the translations and rotations of the interface node are transmitted directly to its surrounding nodes. Figure **??** shows the schematic representation of the interface nodes used for bodies connection: basically, in what follows, they correspond to the center of the linkage joints. Namely, two adjacent bodies are connected by means of the interface nodes, but the bodies do not share other nodes or elements. Consequently, without providing the details of the reduction process (see [30]), the total nodes displacements $\mathbf{u}_i$ can be linked to the coordinates of the interface nodes $\mathbf{u}_{il}$ by a relationship of the form:

$$\mathbf{u}_i = \mathbf{J}_{il}\mathbf{u}_{il} \tag{5}$$

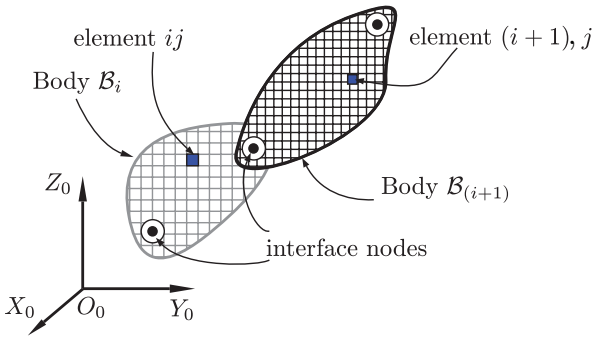

(a) Connection of two bodies by interface nodes

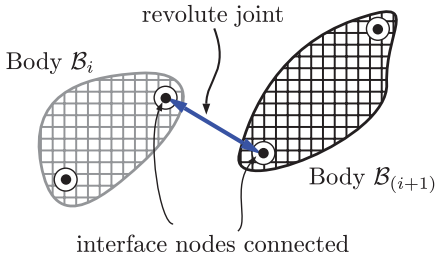

(b) Detail on the interface nodes connection

Fig. 2: Interface nodes for bodies connection

where $\mathbf{J}_{il}$ is a constant matrix.

As a result, the body potential elastic energy after applying static condensation is expressed as:

$$U_{e_i} = \frac{1}{2}\mathbf{u}_{il}^T \mathbf{K}_i^{red} \mathbf{u}_{il}. \tag{6}$$

where $\mathbf{K}_i^{red} = \mathbf{J}_{il}^T \mathbf{K}_i \mathbf{J}_{il}$ is the reduced stiffness matrix associated with the displacements of the interface nodes $\mathbf{u}_{il}$ of the body $\mathcal{B}_i$.

The advantage of using the model reduction technique is quite remarkable. The typical body stiffness matrix usually has a considerable size which depends on the discretization mesh, then using static condensation the body stiffness matrix is compacted into the reduced body stiffness matrix $\mathbf{K}_i^{red}$ with standard size of (6×6) for 2D and (12×12) for 3D (in the case where only two interface nodes per links are used), thus leading to a small stiffness matrix for the assembled linkage.

2.2 Elastostatic model of the linkage

Once the elastostatic model for single body is derived, it is possible to compute the elastostatic model of the linkage. This multibody model considers the linkage configuration and the boundary conditions.

In order to take into account the linkage configuration, the orientation of each body should be considered. Since the reduced body stiffness matrix K_i^{red} is expressed in its own local reference frame, it must be expressed in the global frame, which is done using the coordinates transformation. Therefore, the reduced body stiffness matrix is expressed in the global coordinate system as follows:

$$\left(K_i^{red}\right)_0 = Q_i K_i^{red} Q_i^T \tag{7}$$

where the matrix Q_i is a block-diagonal rotation matrix.

Considering a linkage made of n bodies, as can be seen in Fig. **??**, the full potential elastic energy of the system is given by:

$$\begin{aligned} U_e &= \sum_{i=1}^{n} U_{e_i} = \frac{1}{2}\sum_{i=1}^{n} \left(\mathbf{u}_{il}\right)_0^T \left(\mathbf{K}_i^{red}\right)_0 \left(\mathbf{u}_{il}\right)_0 \\ &= \frac{1}{2} \mathbf{u}_{tot}^{red^T} \mathbf{K}_{tot}^{red} \mathbf{u}_{tot}^{red} \end{aligned} \tag{8}$$

where:

- $\mathbf{u}_{tot}^{red} = \left[\left(\mathbf{u}_{il}\right)_0^T \dots \left(\mathbf{u}_{nl}\right)_0^T\right]^T$ is the vector of interface nodes displacements for all n bodies in the global frame.
- $\mathbf{K}_{tot}^{red}$ is a block-diagonal matrix stacking on its diagonal all bodies stiffness matrices as follows:

$$K_{tot}^{red} = \begin{bmatrix} \left(K_i^{red}\right)_0 & & 0 \\ & \ddots & \\ 0 & & \left(K_n^{red}\right)_0 \end{bmatrix}. \tag{9}$$

The linkage stiffness matrix K_r can be obtained considering the fact that the bodies are connected altogether through the interface nodes. As a result, the expression of the vector $\mathbf{u}_{tot}^{red}$ is derived from a reduced set of independent coordinates $\mathbf{u}_r$, as follows:

$$\mathbf{u}_{tot}^{red} = \mathbf{J}_r \mathbf{u}_r \tag{10}$$

where $\mathbf{J}_r$ is a matrix depending on how the linkage bodies are connected, namely depending on the kinematic relations of the linkage.

The kinematic relations between the interface nodes are defined by the joint type. In the case of the revolute joint, and assuming a rigid connection, all displacements are constrained to be the same, and only the rotation about the joint axis is independent. Thus, considering two adjacent bodies, $\mathcal{B}_i$ and $\mathcal{B}_{(i+1)}$ as we see in Fig. **??**, we have:

$$\mathbf{u}_{tot}^{red} = \left[\mathbf{u}_{il}\ \mathbf{u}_{(i+1)l}\right]^T = \left[\mathbf{u}_{il}^{(1)}\ \mathbf{u}_{il}^{(2)}\ \mathbf{u}_{(i+1)l}^{(1)}\ \mathbf{u}_{(i+1)l}^{(2)}\right]^T \tag{11}$$

If these two bodies are connected by the joints $\mathbf{u}_{il}^{(2)}$ and $\mathbf{u}_{(i+1)l}^{(1)}$, and choosing $\mathbf{u}_{(i+1)l}^{(1)}$ as the dependent coordinates set, the reduced set of independent coordinates is given by:

$$\mathbf{u}_r = \left[\mathbf{u}_{il}^{(1)}\ \mathbf{u}_{il}^{(2)}\ \theta_{(i+1)r}\ \mathbf{u}_{(i+1)l}^{(2)}\right]^T \tag{12}$$

where $\theta_{(i+1)r}$ is the independent coordinate associated with the rotation of body $\mathcal{B}_{(i+1)}$. Furthermore, the boundary conditions related to the linkage supports can be defined using the remaining interface nodes in the reduced set of independent coordinates vector.

Introducing (10) into (8), the potential elastic energy of the linkage is computed by:

$$U_e = \frac{1}{2} \mathbf{u}_r^T \mathbf{K}_r \mathbf{u}_r \tag{13}$$

where the linkage stiffness matrix $\mathbf{K}_r$ is given by:

$$\mathbf{K}_r = \mathbf{J}_r^T \mathbf{K}_{tot}^{red} \mathbf{J}_r \tag{14}$$

Besides, the relation between linkage stiffness matrix, the nodal displacements $\mathbf{u}_r$ and external load $\mathbf{f}_r$ exerted on the linkage joints is given by:

$$\mathbf{f}_r = \frac{\partial U_e}{\partial \mathbf{u}_r} = \mathbf{K}_r \mathbf{u}_r \tag{15}$$

For a linkage with n bodies, the size of $\mathbf{K}_r$ is lower than $(6n \times 6n)$ in the $2D$ case, and for $3D$ case the size is lower than $(12n \times 12n)$.

Equation (15) describes the relation between the external loads acting on the linkage and its joint displacements. By solving this model it is possible to compute the joint displacements in the linkage when it is subject to external loads. This model corresponds to the structural response of the whole linkage, which is used in the optimization process.

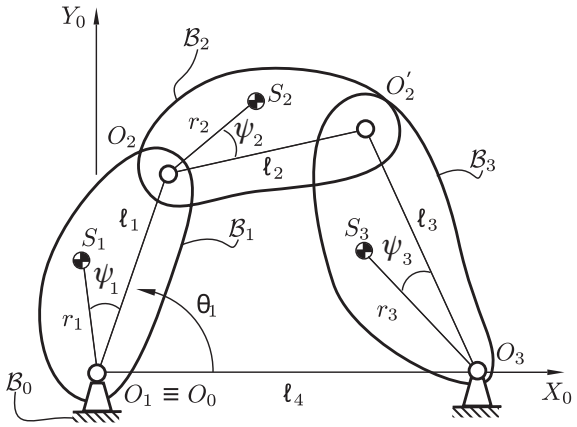

Fig. 3: General scheme of four-bar linkage

In the following section we use the described methodology for multibody topology optimization in order to perform the dynamic balancing of the four-bar linkage. To achieve this goal the four-bar linkage is studied as a flexible multibody system and its dynamic balancing conditions are detailed.

2.3 Reactionless four-bar linkage parametrization

A general scheme of the four-bar linkage is given in Fig. 3. It is composed of three moving bodies $\mathcal{B}_i$, $i = 1, \ldots 3$, and one fixed body, $\mathcal{B}_0$. The mass of body $\mathcal{B}_i$ is m_i, and its length is defined as ℓ_i. The center of mass (COM) S_i of the moving bodies is represented by distances r_1, r_2, r_3, and constant angles ψ_1, ψ_2, and ψ_3, respectively. Furthermore, θ_1 is the angular position of body $\mathcal{B}_1$ with respect to the X_0 axis.

Because the four-bar linkage is modeled using finite elements, each moving body $\mathcal{B}_i$ is discretized in a total of N_i elements, and the element j of the body i is defined by the subscript ij. We define m_{ij} as the mass of the element ij, and x_{ij}, y_{ij} and z_{ij} as the position of the origin M_{ij} of this element in its local frame $\mathcal{F}_i(O_i, x_i, y_i, z_i)$ attached to the body $\mathcal{B}_i$. In Fig. 4 the location of the finite element ij in the body $\mathcal{B}_i$ is represented. It is important to highlight that in this work we perform topology optimization of a planar reactionless four-bar linkage, and the mechanism is consider under planar motions, but the bodies are treated as a three-dimensional ones. The aim of treating the bodies in 3D is to consider the bodies deflections when a general (spatial) load system is applied

Besides, each body can be characterized by its inertial parameters such as its mass, the first moments of inertia, the main moments of inertia, and the products of inertia. The inertia parameters are defined in a local frame

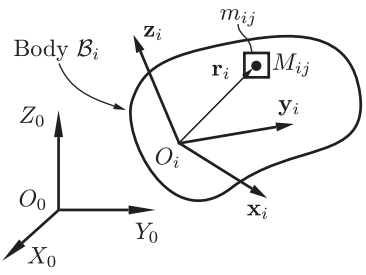

Fig. 4: The finite element ij in the body $\mathcal{B}_i$

rigidly attached to a body, and they do not depend on the linkage configuration. From [39], we have the formulas for the computation of the body inertial parameters. Nevertheless, these formulas must be rewritten as a function of the design variables (element density ρ_{ij}). Considering a linear relation between the mass and the design variable, the following body inertial parameters are obtained:

$$m_i = \sum_{j=1}^{N_i} m_{ij}\rho_{ij} \tag{16a}$$

$$I_{xi} = \sum_{j=1}^{N_i} m_{ij}x_{ij}\rho_{ij}, \; I_{y_i} = \sum_{j=1}^{N_i} m_{ij}y_{ij}\rho_{ij} \tag{16b}$$

$$I_{zzi} = \sum_{j=1}^{N_i} m_{ij}\left(x_{ij}^2 + y_{ij}^2\right)\rho_{ij} \tag{16c}$$

where Eq. (16a) gives the total mass of the body i, while Eqs. (16b) and (16c) are the corresponding static moments and the moment of inertia, respectively.

The balancing conditions to achieve a full dynamic balancing of the four-bar linkage without counterrotations were settled down in the seminal paper [17]. These balancing conditions are based on a set of geometric relations and constraints on the inertial parameters of the links. Indeed, there are three families of this reactionless four-bar linkage, characterized by their links lengths, which are: $\mathbb{S}_1$: $\ell_1 = \ell_4$ and $\ell_2 = \ell_3$, $\mathbb{S}_2$: $\ell_1 = \ell_3$ and $\ell_2 = \ell_4$, and $\mathbb{S}_3$: $\ell_1 = \ell_2$ and $\ell_3 = \ell_4$ [17], which lead to the full dynamic balancing without the use of any counterrotations. The second set of link lengths is depicted in Fig. 5, and this set has proven to be an effective option for design reactionless parallel mechanisms [18, 19]. Therefore, we decided to focus our work on this particular linkage.

The dynamic balancing conditions, given in [17] for the second set of link lengths, must be expressed in a proper manner in order to take into account the elastic model for topology optimization. Following [27], the dy-

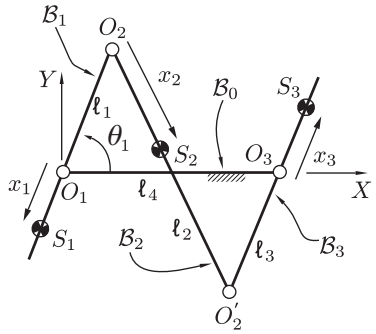

Fig. 5: Dynamically balanced four-bar linkage: Set $\mathbb{S}_2$: $\ell_1 = \ell_3$ and $\ell_2 = \ell_4$

namic balancing conditions are given by:

$$I_{y1} = 0,\ I_{y2} = 0,\ I_{y3} = 0 \tag{17a}$$

$$\frac{I_{x1}}{\ell_1} + m_2 - \frac{I_{x2}}{\ell_2} = 0 \tag{17b}$$

$$\frac{I_{x3}}{\ell_3} + \frac{I_{x2}}{\ell_2} = 0 \tag{17c}$$

$$I_{zz1} - I_{x1}\ell_1 + I_{zz2} - I_{x2}\ell_2 = 0 \tag{17d}$$

$$I_{zz3} - I_{x3}\ell_3 + I_{zz2} - I_{x2}\ell_2 = 0 \tag{17e}$$

Equations (17a) represent the dynamic balancing conditions related to the value of the angles $\psi_1 = \psi_3 = \pi$ and $\psi_2 = 0$ [17]. These conditions preserve the center of mass of each link to be located along its longitudinal axis, as it can be interpreted from the Fig. 3. Note that the inertia parameters of each body are described with respect to the body local frame $\mathcal{F}_i$, whose origin is placed on the joint O_i, with axis x_i along the line which connecting the joints, and the z_i axis is perpendicular to the plane of motion.

3 TOPOLOGY OPTIMIZATION FOR DYNAMIC BALANCING

In this section we report the optimal design of the reactionless four-bar linkage using multibody topology optimization. In the previous sections we described the methodology for linkage modeling, and we presented the dynamic balancing conditions. The optimization process that we will define below, combined with the linkage model presented in the previous section, enables to perform the optimization process for all the linkage bodies simultaneously. The following section is dedicated to the definition of the optimization problem and to its resolution.

Topology optimization for three dimensional multibody systems leads to large scale analysis. Therefore, in order to solve this problem in a reasonable amount of time, a suitable computational platform for fully parallel processing was developed in C++ programming language. It uses the object oriented paradigm and the distributed memory model for parallel computing. This platform is based on the Portable, Extensible Toolkit for Scientific Computation (PETSc) [40], and the platform incorporate some classes provided in [41]. This computational platform is not software dependent, and its results are displayed with ParaView [42]. All the following analyzes were carried out on a computer with a processor AMD Ryzen 9 3900X, using the OS Ubuntu 20.04 64 bits, and PETSc 3.13.3.

3.1 Optimization problem

The four-bar linkage under study was presented in Fig. 5, and the following assumptions are referred to this scheme. The link lengths selected for our studies are: $\ell_1 = \ell_3 = 60\,\text{mm}$, and $\ell_2 = \ell_4 = 200\,\text{mm}$, which are proposed in [27]. The initial design domain for the movable links is presented in Fig. 6. Each link has two joints, which are represented by holes of 4 mm of diameter. Bodies $\mathcal{B}_1$ and $\mathcal{B}_3$ have the same dimensions and thickness of 32 mm, while body $\mathcal{B}_2$ has 10 mm of thickness. The initial dimensions of the links were defined after several simulations, choosing the design/solution with less material between the joints, but with a meaningful design. This implies to have links with bigger thickness. Performing specific analysis in order to select the dimensions of these initial guesses can be a particular topic of study, which is out of the scope of our paper.

The assembled linkage is subjected to external loads which are applied, with respect of the global frame, as follows (see Fig. 5): at O_2 and O_2' a force equal to $f = [10,\ 10,\ 10]^T$ N, applied along the x, y and z global axes. Additionally a moment at O_3 of 1 Nm is applied around z-axis, while the joint O_1 is fixed at $\theta_1 = \pi/2$.

The approach consists of generating a mesh for each body and analyzing them as a multibody system under a set of loads and boundary conditions, such as it was described in Section 2. The mesh is generated as a structured 3D grid using 8-node linear hexahedral elements. The finite element (FE) analysis is assumed linear elastic, and a penalization factor for the SIMP scheme equal to $p = 3$. The element size is equal to 2 mm for all bodies and each node has three degree of freedom for Cartesian displacements. Hence, the four-bar linkage is modeled using a total of 116,789 elements and it generates a FE model with 362,700 degrees of freedom.

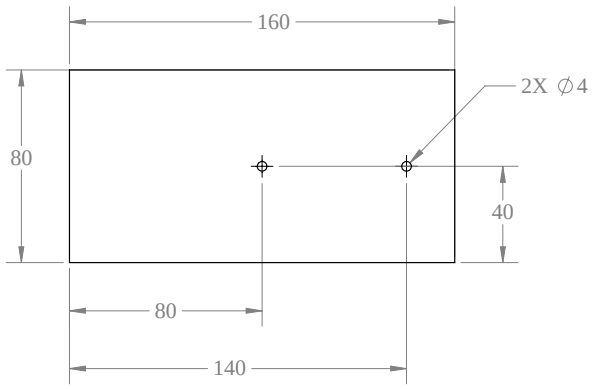

(a) Initial design domain of bodies $\mathcal{B}_1$ and $\mathcal{B}_3$

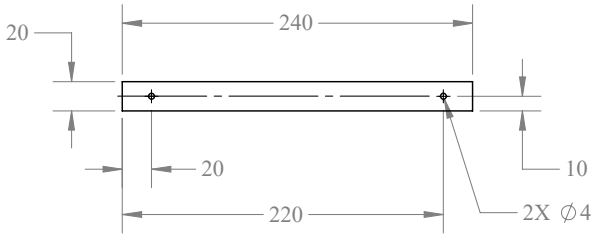

(b) Initial design domain of body $\mathcal{B}_2$

Fig. 6: Initial design domain of four-bar links. All dimensions are in millimeters

In order to model a link we use passive and active elements. Both types of elements are considered in the finite element analysis, but only the active ones are included in the optimization process. Namely, the density of passive elements never changes, and their initial state can be zero or one (void or solid).

In our case, we use passive elements with the purpose of modeling the link joints. A void region is used to create the hole in the joint, and the solid region represents the material required to create the joint. This solid region is considered in the computation of inertial parameters.

As is usual in topology optimization problems, we apply a filtering procedure in order to obtain a layout without checkerboard problem. This filter modifies the density variables based on the density of their neighborhoods, it is know as density filter and was proposed in [43].

Additionally, we study how materials combination with different densities affects the mechanism footprint. In our study, we consider the mechanism footprint to be defined as the volume occupied by the mechanism, i.e., the total volume of the links. For this purpose, we consider to include in links $\mathcal{B}_1$ and $\mathcal{B}_3$ a cylinder made of steel, while the link is made of material with lower density. Thus, using the cylinder of steel, the link volume should be smaller compared with a link made of the same material but without the cylinder.

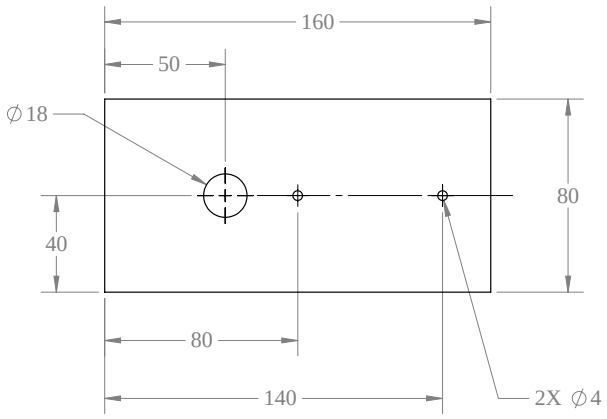

Fig. 7: Initial design domain of bodies $\mathcal{B}_1$ and $\mathcal{B}_3$ when the cylinder is included. All dimensions are in millimeters

Hence, we performed four optimization processes for different links materials, and they are as follows:

- Case I: All the links are made of nylon.
- Case II: All the links are made of aluminium.
- Case III: All the links are made of nylon and bodies $\mathcal{B}_1$ and $\mathcal{B}_3$ includes a cylinder of steel.
- Case IV: All the links are made of aluminium and bodies $\mathcal{B}_1$ and $\mathcal{B}_3$ includes a cylinder of steel.

For case III and IV, the bodies $\mathcal{B}_1$ and $\mathcal{B}_3$ have a hole to contain a cylinder, as can be seen in Fig. 7. The cylinder has diameter of $18\,\mathrm{mm}$ and it length is $32\,\mathrm{mm}$, thus its mass is $63.5\,\mathrm{g}$. The cylinder of steel only affects the inertial parameters and total mass of the links, which are considered in the optimization process. Indeed, the cylinder is only a rigid body included in the FE model, but its shape, density and location cannot be modified by the topology optimization procedure. The cylinder should help reducing the total footprint of the links due to the higher density of the material. The material properties used for the optimization process are summarized in Table 1.

3.2 Definition of the optimization problem

In order to prevent negative effects due to excessive deformations, such as wear, low accuracy, and even vibrations, we decide to optimize the linkage stiffness. For this purpose, it is decided to minimize the strain energy

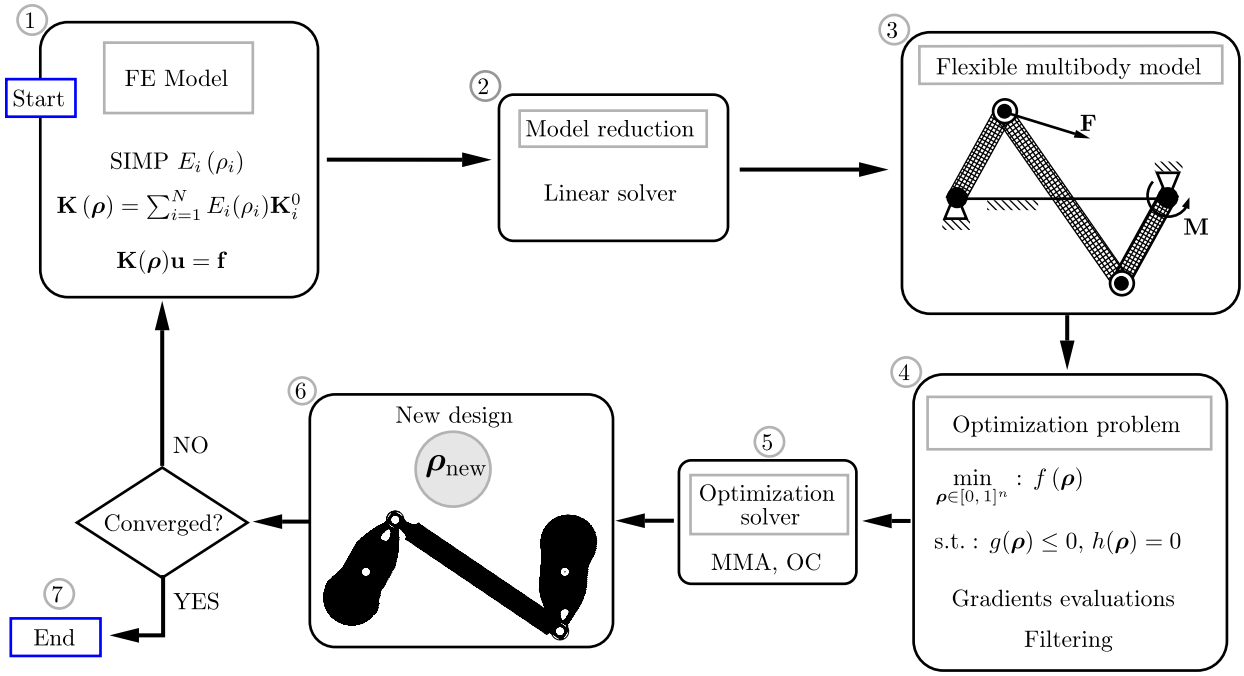

Fig. 8: Structural topology optimization process for flexible multibody systems

Table 1: Material properties

Material	**Density** [kg/m^3]	E_0 [GPa]	**Poisson ratio**
Nylon (PA66)	1150	2.76	0.39
Aluminium	2700	68.9	0.33
Steel	7800	210	0.3

stored in the structure under a given loading, i.e. to minimize the compliance (or to maximize stiffness). Indeed, compliance is a standard objective function for structural topology optimization and it is used in many research works [26]. Therefore, compliance is established as the objective function, and it is minimized while constant load is applied, under dynamic balancing constraints.

The set of balancing conditions given in Eq. (17) are essentially equality constraints, but they are transformed into inequalities in order to avoid a very restrictive optimization scheme. It is done by replacing the equality constraint $h = 0$, with two inequality constraints, $h - \epsilon \leq 0$ and $-h + \epsilon \leq 0$, where ϵ is a small number called relaxation parameter. Therefore, after generating the inequalities, there are twice number of balancing conditions. This relaxation procedure is a mathematical trick used in order to replace an equality sometimes hard to maintain or to reach by an optimization solver by two opposite inequalities.

Consequently, the mathematical formulation for the optimal design of a reactionless four-bar linkage is expressed as:

$$\begin{aligned} &\min_{\boldsymbol{\rho}\in[0,1]} : f(\boldsymbol{\rho}) = u_r^T K_r u_r \\ &\text{subject to} : g(\boldsymbol{\rho}) \leq 0 \end{aligned} \tag{18}$$

where the compliance is computed using the linkage stiffness matrix K_r, and u_r is the reduced set of independent coordinates, both given in Eq. (15). Moreover $g(\boldsymbol{\rho})$ is the set of dynamic balancing conditions expressed as inequalities constraints. Besides, the objective function and the constraints are normalized using their values computed for the first iteration, excluding Eq. (17a) whose initial values are null. Note that both objective and constraints in the optimization problem (18) are computed for the entire linkage, imposing that all links are optimized in the same time by the TO solver.

On the other hand, the problem we face is characterized by a high number of variables, typically greater than 10^5 in our examples. In order to solve the optimization problem it is necessary to use an optimization solver (optimizer), with capacity to handle large number of variable, as well as multiple constraints. Thus, the method of moving asymptotes (MMA) introduced in [44] is the

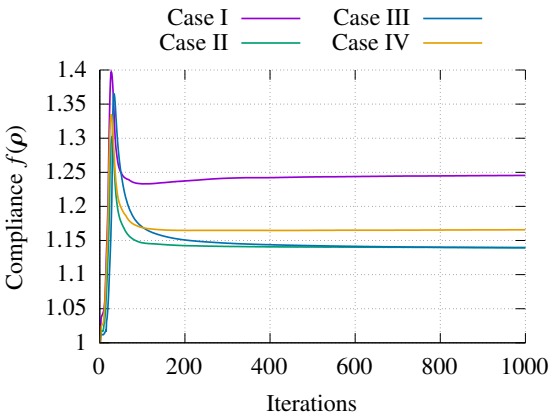

Fig. 9: Compliance evolution of the four cases

Table 2: Optimal solutions

Case	**Time** [h]	**Max. const. violation** [%]	$f(\rho)$
I	23.63	$6.64 \cdot 10^{-4}$	1.24
II	20.91	$1.09 \cdot 10^{-4}$	1.16
III	23.05	$1.69 \cdot 10^{-4}$	1.13
IV	20.94	$1.13 \cdot 10^{-4}$	1.13

optimizer used for this research work. It is able to handles multiple inequality and equality constraints, and is the most accepted optimizer in the structural optimization community because of its excellent convergence properties [26]. The parallel implementation of this method is provided in [41]. Additionally the schematic representation of the general optimization process is depicted in Fig. 8. Even if the figure illustrates the mechanism to be optimized by depicting the four-bar linkage, the procedure of our proposed approach is applicable for any general multibody system.

It should be noted that the MMA requires to provide the analytical expressions of the gradients of the objective function, as well as its constraints. The gradients are derived analytically, and then included in the optimization algorithm [30]. It is important to point out that the dynamic balancing conditions, used as a constraints, are linear with respect to the decision variable, which simplifies the gradient computation.

3.3 Numerical results

In our case, constraint violation is defined as an index to evaluate the fulfillment of the dynamic balancing conditions. Hence, because of optimization problem behavior is monotonic when approaching convergence, the stopping criteria (convergence criterion) is defined based on the number of iterations. Whereby the optimization process was run for each case until it reached 1000 iterations, in such a way that it is ensured a lowest constraints violation. The constraints are normalized using their values for the initial design, thus the constraint violation percentage is computed based on the initial and final values of the constraints.

The optimal solutions are summarized in Table 2, where the computation time, maximum constraint violation and objective function values are displayed for each case. The values of the constraint violation shows that the constraints are properly satisfied. Besides, the objective function evolution is shown in Fig. 9 for the four cases, where it can be seen that the algorithm is properly converging.

The next section provides the results after perform the multibody topology optimization for the dynamic balancing of the four-bar linkage. The finite element model, loads, boundary conditions, objective function, and constraints are the same for all study cases, the only difference is the material used in each case.

4 RESULTS

The results from our topology optimization procedures are essentially structured meshes, where all the elements are hexahedral of the same size, as it is shown in Fig. 10. These type of results are known as a voxel-based results. Figure 10a presents the results corresponding to the body $\mathcal{B}_1$, where it shows a density field which ranging from 0 to 1, and its corresponding colors are blue and red, respectively. A section view of the link $\mathcal{B}_1$ is presented in order to visualize its internal part, which can be seen in Fig. 10b. Finally, Fig. 10c was generated after applying a filter to remove the elements with density below 0.95.

In the following sections we examine the linkage footprint reduction comparing the four described cases. Then, we describe and analyze the linkage optimized properties focusing on the results of Case I. Numerical validations corresponding to the linkage compliance and dynamic balancing were carried out using commercial specialized software such as ANSYS and ADAMS, respectively.

Considering the results from Case I, we built a prototype in order to evaluate by an experiment the dynamic balancing of the optimized linkage. Details on the manufacturing process and experimental setup are described at the end of the section. Besides, the audiovisual material is provided alongside the manuscript.

It is worth mentioning that the links shape obtained

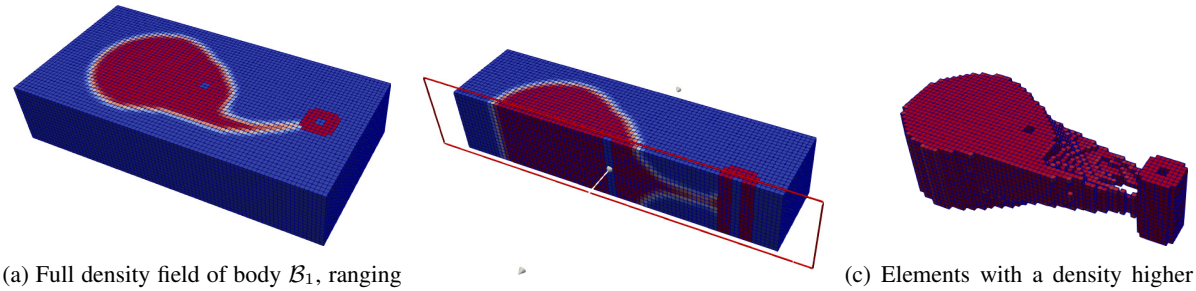

(a) Full density field of body $\mathcal{B}_1$, ranging from 0 to 1

(b) Internal section view

(c) Elements with a density higher than 0.95

Fig. 10: Voxel-based results of body $\mathcal{B}_1$ for Case I

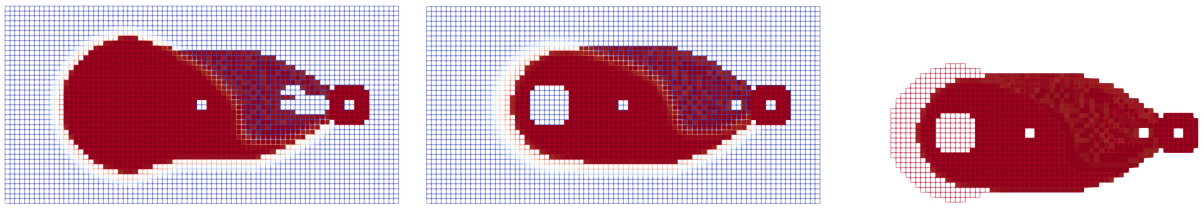

(a) Case I: Optimized body $\mathcal{B}_1$

(b) Case III: Optimized body $\mathcal{B}_1$ with cylinder

(c) Overlapping of results: Case I and III

Fig. 11: Linkage footprint comparison

for the optimization problems that we define are valid only for those particular problems. While the optimized dynamic balancing properties are valid for the general linkage configuration, the structural properties are optimized for the given linkage configuration.

4.1 Linkage footprint reduction

Based on the optimization results, we can consider, for a practical point of view, that the optimized bodies can generate a bulky mechanism. Thus, in order to reduce the footprint of the mechanism, we carried out the optimization process for different material combinations, described as a Case I, Case II, Case III, and Case IV.

We decide to use the volume of the bodies as an index to evaluate the linkage footprint reduction. The volume of each body is computed from the voxel-based results of the optimization process, it means that we evaluate the volume of the body taking into account the elements with a density higher than 0.95. The results of the optimization Cases I and III are presented in Fig. 11. In these figures we show only body $\mathcal{B}_1$ for all optimization cases, but the volumetric reduction is computed for the entire linkage.

Fig. 11a shows the optimized body $\mathcal{B}_1$ from Case I. If we analyze the same problem, but including now a cylinder of steel (Case III), then we obtain the body shown in Fig. 11b. In addition, in order to compare the differences of using a material with higher density, the overlapping meshes are presented in Fig. 11c. The volumetric reduction when Case I and Case III (including the cylinder hole) are compared is $11.21\ \%$. Besides, the volumetric reduction when Case II and Case IV (including the cylinder hole) are compared is $7.44\ \%$.

From the described results, we can conclude that the cylinder works as a counterweight, and at the same time, due to its high density less material is required to achieve dynamic balancing in bodies $\mathcal{B}_1$ and $\mathcal{B}_3$. Indeed, the dimensions and location of the cylinder should be optimized for an optimum footprint reduction, which is left as a future work. For our examples, we define the dimensions and location performing several simulations, choosing the dimensions and location that produced results that converge to meaningful designs in all cases.

4.2 Numerical validations

The optimization results that have been presented cannot be treated as a solid object in standard Computer-Aided Design (CAD) software. In order to have an editable CAD file, it is mandatory to perform a body-fitted post-processing, i.e., to convert the voxel-based results to a smooth design suitable for a CAD software. Using Paraview we apply some filters in order to generate a triangular mesh which can be exported to STL file. The STL

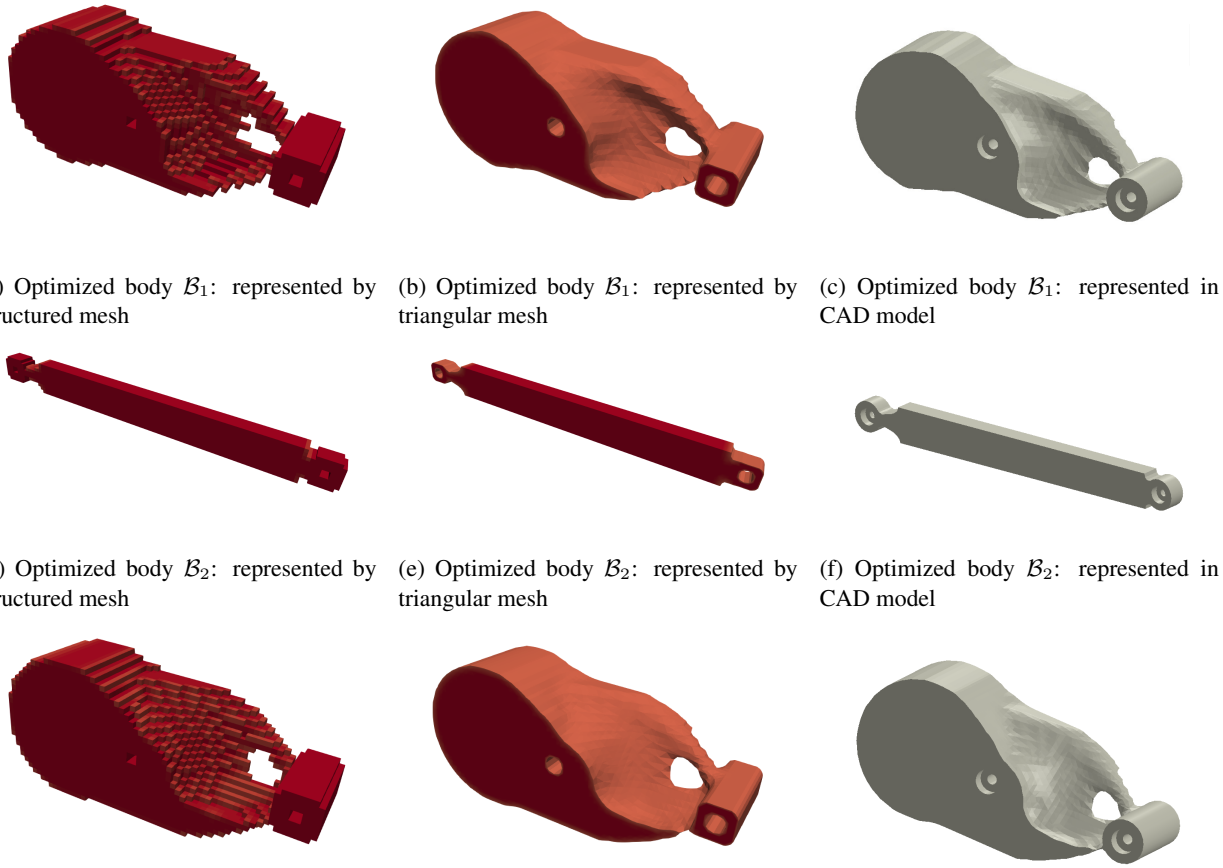

(a) Optimized body $\mathcal{B}_1$: represented by structured mesh

(b) Optimized body $\mathcal{B}_1$: represented by triangular mesh

(c) Optimized body $\mathcal{B}_1$: represented in CAD model

(d) Optimized body $\mathcal{B}_2$: represented by structured mesh

(e) Optimized body $\mathcal{B}_2$: represented by triangular mesh

(f) Optimized body $\mathcal{B}_2$: represented in CAD model

(g) Optimized body $\mathcal{B}_3$: represented by structured mesh

(h) Optimized body $\mathcal{B}_3$: represented by triangular mesh

(i) Optimized body $\mathcal{B}_3$: represented in CAD model

Fig. 12: Post-processing of the optimized four-bar mechanism of Case I

format usually can be read by any standard CAD package, and then the CAD program converts the STL file into its native format. These changes are necessary in order to create an adequate CAD model for the physical prototype and numerical validations. Figure 12 shows the post-processing from voxel-based results to CAD models, corresponding to the links of the optimized reactionless four-bar linkage of Case I. It should be noted that the optimized shapes of links $\mathcal{B}_1$ and $\mathcal{B}_3$ have only slight differences, even if they are not constrained to be equal. The shapes obtained for these links are necessary bulky due to the necessity to have material on their left-hand side in order to counterbalance the mass on the other side. On the right-hand side, the obtained shape of the links $\mathcal{B}_1$ and $\mathcal{B}_3$ is well appropriate for resisting to bending effects in all directions. Regarding the link $\mathcal{B}_2$, this link is subject to tension/compression only, which explains its shape.

The optimized properties of the four-bar linkage are the compliance and dynamic balancing. Hence, in order to validate these properties, the compliance is evaluated using ANSYS, and the dynamic balancing of the linkage is analyzed with ADAMS. For this purpose the results from Case I are considered. In Table 3 the inertial properties of the optimized reactionless four-bar linkage are presented, where the center of mass location along X_i-axis x_i, the static moment of inertia (I_{xi}) and the moment of inertia (I_{zzi}) are defined with respect to the body local frame $\mathcal{F}_i$. Because of the balancing conditions given in Eq. (17a), the value of the static moment I_{y_i} of each optimized body is $I_{y_i} \approx 0$ and consequently, are not displayed in Table 3.

Using the inertia properties of the bodies given in Table 3, the balancing conditions can be verified: Eqs. (17b,c) are of magnitude 10^{-3}, Eq. (17d) of magnitude 10^{-4} and Eq. (17e) of magnitude 10^{-5}, i.e. in all case all equations are much smaller than the amplitude of

Table 3: Properties of the optimized reactionless four-bar linkage (Case I)

$\mathcal{B}_i$	ℓ_i [m]	m_i [kg]	x_i [m]	I_{xi} [kg·m]	I_{zzi} [kg·m^2]
1	0.06	0.13480	-0.01241	-1.6735·10^{-3}	1.5740·10^{-4}
2	0.2	0.04484	0.10278	4.6086·10^{-3}	6.2334·10^{-4}
3	0.06	0.13367	-0.01217	-1.6280·10^{-3}	1.5642·10^{-4}

Table 4: Joint deformations (meters)

Joint	ANSYS			
	X	Y	Z	Norm
O_2	$4.36 \cdot 10^{-5}$	$2.55 \cdot 10^{-9}$	$8.85 \cdot 10^{-6}$	$4.45 \cdot 10^{-5}$
O_2'	$3.69 \cdot 10^{-5}$	$-2.50 \cdot 10^{-5}$	$4.49 \cdot 10^{-6}$	$4.48 \cdot 10^{-5}$
	Computational platform			
	X	Y	Z	Norm
O_2	$4.30 \cdot 10^{-5}$	$2.48 \cdot 10^{-9}$	$4.10 \cdot 10^{-6}$	$4.32 \cdot 10^{-5}$
O_2'	$3.66 \cdot 10^{-5}$	$-2.37 \cdot 10^{-5}$	$4.78 \cdot 10^{-6}$	$4.39 \cdot 10^{-5}$

the terms involved in them, meaning that the balancing conditions are valid.

4.2.1 *Compliance validation*

The objective function was defined as the compliance, and it was minimized in order to ensure the stiffest linkage design. With the aim to verify the results obtained with the proposed approach, we perform a numerical validation of the linkage compliance using ANSYS.

The numerical validation with ANSYS is based on the static structural analysis of the linkage. It was carried out using the conditions described in the optimization problem definition. Since the compliance is twice the strain energy, considering the strain energy computed with ANSYS, the compliance can be obtained by adding up the strain energy of all elements. In the optimization process we normalize the objective function, but in order to compare the values, a non-normalized compliance value is used. The compliance value from the optimization procedure is $1.8346 \cdot 10^{-3}$ J, and the ANSYS compliance value is $1.8469 \cdot 10^{-3}$ J, based on these results we obtain a small error of 0.6704 %.

Even though the aim of this work is not to perform an intensive linkage structural analysis, it is necessary to verify the structural integrity of the linkage for the described conditions. Thus, the total deformations were analyzed in ANSYS, having a maximum total deformation of $5.37 \cdot 10^{-5}$ m. The total deformation plot is shown in Fig. 13, where deformations are scale excessively for display purposes.

Besides, Table 4 summarizes the computed joint deformations using ANSYS and the corresponding deformations obtained with the optimization framework. From Table 4, and considering the ANSYS results, the maximum joint displacement occurs at the joint O_2'. The linkage has a less stiff behavior when is analyzed in ANSYS, nevertheless the comparative error for the joints deformation is very low, having a value of 2.96 % for joint O_2, and 1.94 % for joint O_2'. In general, these results agree with the compliance validation, the higher strain energy is due to larger deformations when a constant load is applied.

Differences in the comparative analyses arise from the particularities in each finite element model. In ANSYS, we use the CAD model obtained after file format conversions, and the mesh is generate using the hex dominant method with the option of low order elements (linear hexahedral), but due to the complex shape of the links, in some regions tetrahedral elements appears. In our optimization program we use structured mesh with hexahedral elements. Thus, we do not expect to have equal values, but very similar ones as they are shown.

4.2.2 *Validation of dynamic balancing*

Numerical validation of the dynamic balancing was carried out using the ADAMS software. In order to analyze the results, the optimized model is compared with an unbalanced four-bar linkage. This unbalanced linkage has been modeled with the same links length and mass as the optimized links, but with the center of mass placed between joints for each link.

The reactions loads on the base, for the balanced and unbalanced linkages, have been simulated for arbitrary motions. The input angular velocity in the body $\mathcal{B}_3$ is a sinusoidal function equal to $0.37\sin(\pi t)$, and the gravity is not considered. In Fig. 14 the corresponding results of balanced and unbalanced models are presented. The Fig. 14a shows the corresponding reaction force of balanced and unbalanced linkages. With respect to the shaking moments, the reaction moment for the dynamic balanced linkage and unbalanced one is shown in Fig. 14b. The computed reaction forces and moments clearly demonstrate the dynamic balancing of the four-bar linkage.

In addition, in Table 5 we present a comparison between the balanced and unbalanced linkages, taking into account the RMS of the reaction loads. The body-fitted post-processing produces numerical errors which generate the very small unbalance in the linkage. These numerical errors can be reduced using a finer mesh, but finer mesh lead to a huge computational cost, which is not jus-

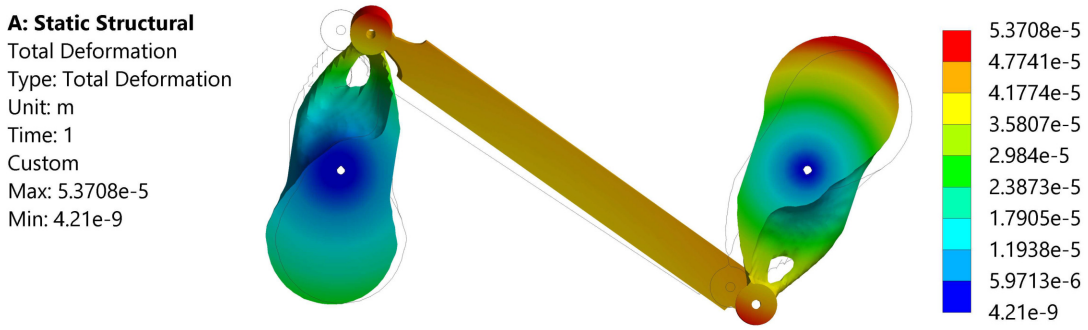

Fig. 13: Total nodal coordinate change map using ANSYS

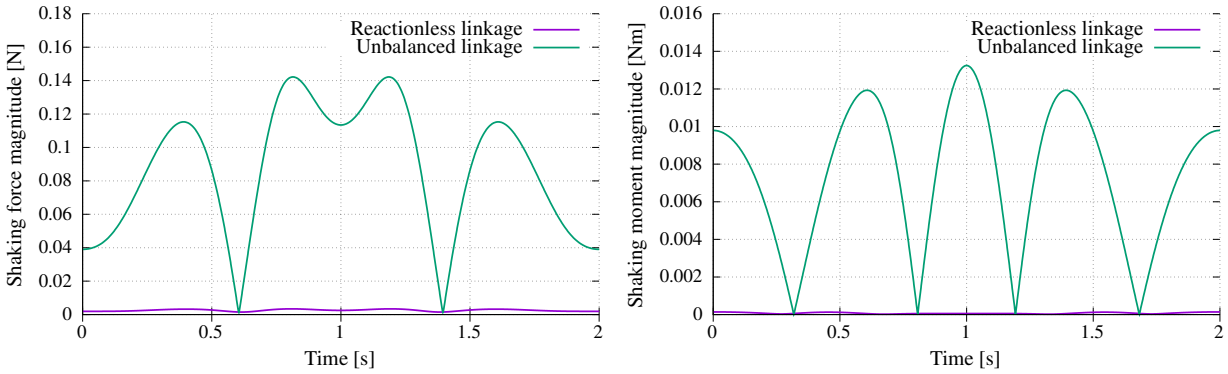

(a) Comparative shaking force

(b) Comparative shaking moment

Fig. 14: Numerical validation of dynamic balancing using ADAMS

Table 5: Reaction loads comparison using their RMS values

Reaction load (magnitude)	Unbalanced	Reactionless	Reduction (%)
SF [N]	0.0951	0.0026	97.26
SM [Nm]	0.0083	$8.46 \cdot 10^{-5}$	98.98

tified in our case due to the small remaining balancing errors.

4.3 Prototype

Because of the complex shapes generated with topology optimization, the best option to fabricate the optimized bodies is the Additive Manufacturing (AM) technique. Nevertheless, there are some situations where the optimization parameters generates shapes, which can be fabricated with traditional manufacturing techniques.

In our optimization problems, the applied loads affects considerably the resultant shapes. If the applied load in Case I is replaced with a force equal to $f = [1,\ 1,\ 1]^T$ N (ten times smaller than the original), some cavities begin to emerge in the optimized bodies, what makes impossible to fabricate the links with traditional manufacturing techniques. In Fig. 15, the optimization results based on this modified Case I are presented, and as we can appreciate in Fig. 15b, the body has cavities.

For the load conditions that we defined in our optimization problems, the resultant shapes do not present internal hollows. Thus, the prototype presented in this work was manufactured with a CNC milling machine, using the optimized design of the Case I. The CAD model and the physical prototype are shown in Fig. 16. For the physi-

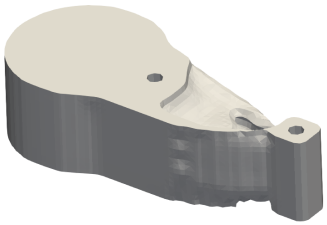

(a) Optimized body

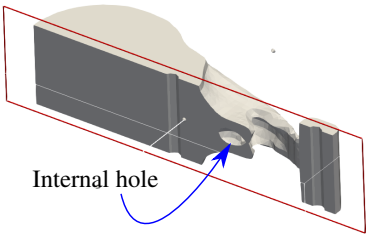

(b) Section view with cavities

Fig. 15: Cavities in an optimized body

cal realization (not for numerical validations), the link $\mathcal{B}_2$ was divided in two parts in order to avoid link collisions, while keeping the balancing conditions unchanged.

4.3.1 Prototype performance

In order to verify the dynamic balancing of the optimized linkage, experimental tests were carried out. The purpose is to evaluate the effects of the residual shaking force and moment in the case of the dynamically balanced linkage. The experimental setup consists in a fixed structure, the linkage base and the cables. Hence, the base of the linkage was suspended from the fixed structure with four cables, as it can be seen in Fig. 17. This arrangement allows the linkage to move freely in the presence of unbalanced reaction loads. We use a direct current motor to provides oscillating movement in the linkage, which is attached to body $\mathcal{B}_3$.

With the aim of studying the prototype performance, we record with a camera the location of the suspended base during the linkage motion, and the resultant oscillatory motion is analyzed using video processing[1]. Indeed, the amplitude of the oscillatory motion of the platform can be related to the amplitude of the shaking force and shaking moment exerted by the moving linkage: the smaller the motion, the smaller the unbalance effects. This will be discussed below. For this task, we use the open source software called Tracker [45], which is an image and video analysis package. Besides, in order to compute the linkage base displacements, it is fundamental to define an inertial reference frame, calibrate the video scale, and designate the feature to be tracked. The video scale is the ratio of a real dimension to an image dimension in pixels between two points, and it is computed providing the real dimension of an object in the video.

As it can been seen in Fig. 17, the linkage is recorded from the top-view. The home position is defined by the reference frame XY shown in Fig. 18, and it remains fixed while the mechanism is in motion. We define the bearing on the joint O_1 as the feature of interest, this feature will be tracked in the video during the motion of the linkage. Therefore, using the position of the tracked feature based on the reference frame, the linkage translations were determined. Besides, the platform rotation is computed around the Z-axis, using the translation of two features belonging to the linkage.

The experiments were performed for two scenarios, as we can see in Fig. 18. In the first scenario, we use the optimized linkage to observe its behavior, Fig. 18a. Then, for the second scenario we attach an extra mass ($46.5\,\mathrm{g}$) on the body $\mathcal{B}_2$ in order to induce an unbalance. This mass is placed near to the joint O_2, that can be seen in Fig. 18b. For the two scenarios we use the same input motion equals to $\cos(1.6\pi t)$, which is generated by the DC motor attached to body $\mathcal{B}_3$.

In Fig. 19 we present a comparative evolution of the computed displacements for the first and second scenarios. In Fig. 19a, the magnitude of the displacements for the balanced linkage are presented, and the corresponding displacements for the unbalanced case are given in Fig. 19b. The platform rotation is shown in Fig. 19c for the balanced linkage, and the Fig. 19d shows the respective platform rotation for the unbalanced linkage.

From the experimental results, we can observe small translations and rotations in the case of the balanced linkage, which implies that there are residual unbalanced reaction loads. These unbalanced reaction loads can be the consequence of numerical errors, generated when the file format conversions were made, and of course due to the errors generated for the manufacturing process, and because of the quality of the mechanical components. Nonetheless, if we compare the first and second scenarios, the transnational displacement reduction based on their RMS values is $85.48\ \%$, having a maximum translation of $1.16 \cdot 10^{-3}\,\mathrm{m}$ for balanced case, and $6.77 \cdot 10^{-3}\,\mathrm{m}$ for unbalanced one. Regarding to the platform rotation, we can find a maximum absolute value of $0.42\,\mathrm{deg}$ when the mechanism is dynamically balanced, and a maximum rotation of $3.36\,\mathrm{deg}$ for the unbalanced case, these results

[1] A movie of the camera records is available here: https://uncloud.univ-nantes.fr/index.php/s/xfzrJMipy6zJAYN

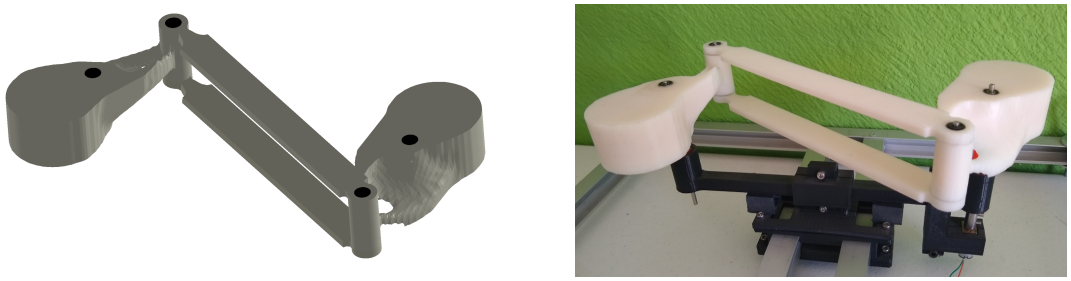

(a) CAD model (b) Physical prototype

Fig. 16: Prototype of the optimized reactionless four-bar linkage

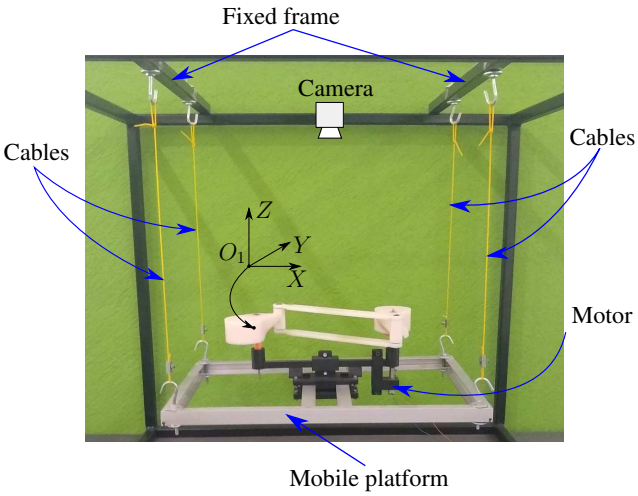

Fig. 17: Experimental setup for the dynamically balanced four-bar linkage

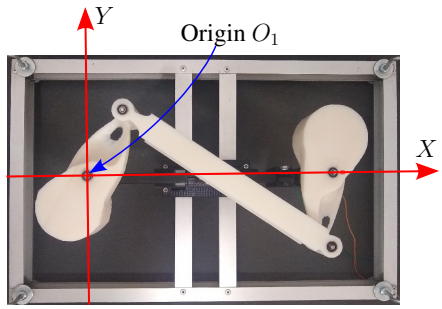

(a) Dynamically balanced four-bar linkage

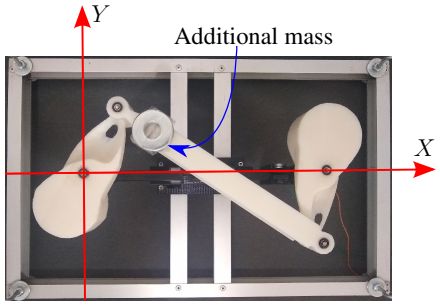

(b) Four-bar linkage with additional mass

Fig. 18: The four-bar linkage in its home position for the two scenarios

lead to a reduction of 89.26 % with respect of their RMS values.

In order to analyze more these results, let us mention that the lengths of the cables are identical in the balanced and unbalanced case (1 meter), and that the change in the mass of the device supported by the cables varies by 5 % from the balanced (860.7 g) to the unbalanced case (907.2 g). As a result, the eigenfrequencies of both systems should be barely the same: this can be observed by doing a FFT of the signals obtained by the camera. We obtained the following frequencies for both systems:

- First oscillating frequency: of 0.50 Hz; This frequency is indeed the pendulum frequency $\sqrt{g/\ell}/2/\pi$, with $g = 9.81\ \mathrm{m/s^2}$ and $\ell = 1\ \mathrm{m}$.
- Second oscillating frequency of 0.88 Hz; This frequency is the frequency of oscillation of the device around a vertical axis.

These results showed that the oscillation frequencies of the pendulum are not impacted by the changes in mass.

The change of the device motion's amplitude is thus necessary due to the change of the solicitations made by the mechanism on the cables. We tested several types of input motions and several cable lengths, and in every case, the unbalanced mechanism lead to large motions of the suspended device, contrary to what happened with the balanced linkage. Because this appears for several solicitations made by the linkage on the cables as well as for several cable lengths, we may thus conclude that the

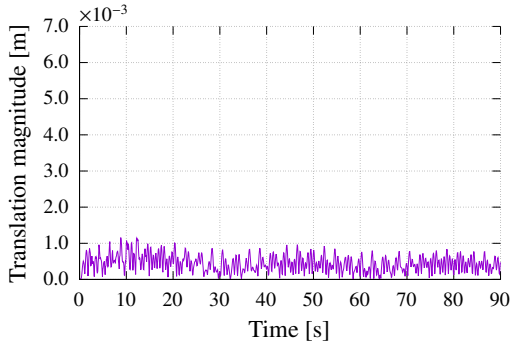

(a) Balanced four-bar linkage translation on XY plane

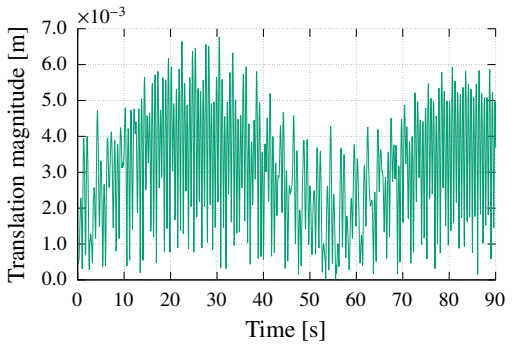

(b) Unbalanced four-bar linkage translation on XY plane

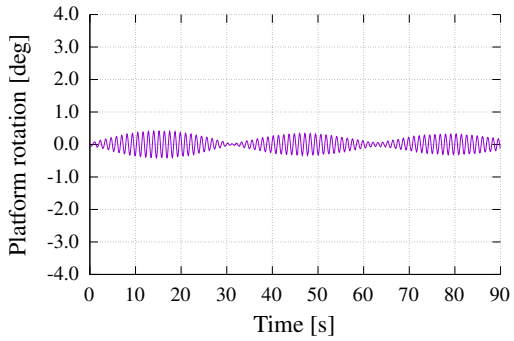

(c) Balanced four-bar linkage rotation around the Z axis

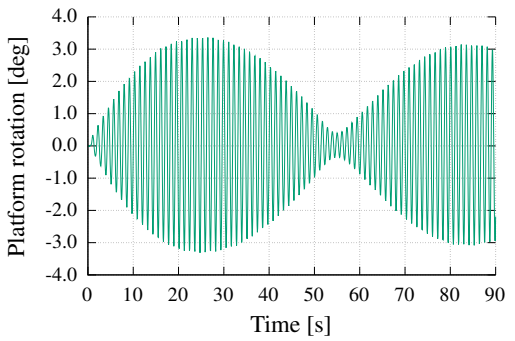

(d) Unbalanced four-bar linkage rotation around the Z axis

Fig. 19: Experimental platform displacements for the balanced and unbalanced four-bar linkages

larger amplitudes are related to larger shaking forces or moments applied by the unbalanced mechanism.

All these results show that, by using TO, we were able to design a reactionless four-bar linkage while taking into account its elastic behavior during the design process. Note that a movie showing the frame's motion for the balanced and unbalanced cases is provided in the attached multimedia content.

5 CONCLUSIONS

The research work described in this paper demonstrated the feasibility and reliability of using structural topology optimization as a tool for linkage design under balancing constraints. Indeed, we have shown that dynamic balancing conditions can be fulfilled while the link elasticity is considered.

In our research, the numerical validation of the reactionless four-bar linkage evinced an excellent dynamic balancing performance. The residual shaking forces and moments, that appeared in the simulation, were generated because of the body-fitted post-processing, but this unbalance was almost negligible. The dynamic balancing performance of the optimized four-bar linkage was numerically validated using ADAMS. The shaking force and moment reduction is $97.26\ \%$ and $98.98\ \%$, respectively. This paper is the first work that explores numerical validation of the dynamic balancing behavior of an optimized linkage generated with structural topology optimization.

Even if our main objective was not to perform an intensive structural design, in order to take into account the link elasticity, we optimized the linkage stiffness through minimizing the compliance. In this way, we avoided excessive deformations, which are source of low accuracy, wear and even vibrations. The linkage compliance was validated with the commercial software ANSYS. The comparison between the optimized compliance value and the compliance obtained with ANSYS by structural analysis has an error of $0.6704\ \%$. This small error indicated that the optimization was successfully performed.

A prototype was built, and its dynamic balancing performance was analyzed using video processing, wherewith the effects of the residual shaking force and moment were evaluated. These effects are embodied as translations and rotations on the base of the optimized linkage, which were measured and compared with those of an un-

balanced linkage. The experimental displacements of the optimized linkage, compared with the unbalanced one, are clearly reduced. This simple, but enlightening experiment, allowed to evaluate the dynamic balance of the optimized linkage beyond a numerical validation. Hence, comparing the balanced and unbalanced scenarios, the translational displacement reduction based on their RMS values is $85.48\ \%$, while the reduction in the platform rotation is $89.26\ \%$.

It is worth to clarify that the presented results were obtained in a computational framework specially designed for the multibody topology optimization problem. This framework is software independent, written in C++ programming language using the object oriented paradigm, and it is based on the distributed memory model for parallel computing. In consequence, this computational platform has the potential to solve large-scale problems, despite the fact that the results presented here were obtained on a desktop computer.

The dynamic balancing of multibody systems using structural topology optimization is a novel approach which has several potential directions to be explored. The optimization of robotic mechanisms with more degrees of freedom (planar/spatial), for a set of critical trajectories is envisaged.

6 ACKNOWLEDGMENTS

The first author wishes to acknowledge the scholarship received from CONACYT (National Science and Technology Council, Mexico) for his PhD studies.

REFERENCES

[1] Lowen, G. G., and Berkof, R. S., 1968, "Survey of investigations into the balancing of linkages," *Journal Mechanisms,* **3**, pp. 221–231.

[2] F.R.E. Crossley, 1954, *Dynamics in Machines* Roland Press, New York.

[3] Berkof, R. S., and Lowen, G. G., 1969, "A new method for completely force balancing simple linkages," *Journal of Engineering for Industry,* **91**(1), pp. 21–26.

[4] Berestov, L.V., 1977, "Comparative analysis of the reactions in the kinematic pairs of the four-bar linkages for the different balancing methods," *Russian Journal "Mekhanika Machin"*, pp. 61–70.

[5] Kochev, I. S., 2000, "General theory of complete shaking moment balancing of planar linkages: a critical review," *Mechanism and Machine Theory,* **35**(11), pp. 1501–1514.

[6] Arakelian, V. H., and Smith, M. R., 2008, "Design of planar 3-DOF 3-RRR reactionless parallel manipulators," *Mechatronics,* **18**(10), pp. 601–606.

[7] van der Wijk, V., Demeulenaere, B., Gosselin, C., and Herder, J. L., 2012, "Comparative analysis for low-mass and low-inertia dynamic balancing of mechanisms," *Journal of Mechanisms and Robotic,* **4**(3).

[8] Kamenskii, V. A., 1968, "On the question of the balancing of plane linkages," *Journal of Mechanisms,* **3**(4), pp. 303–322.

[9] Agrawal, S. K., and Fattah, A., 2004, "Reactionless space and ground robots - novel designs and concept studies," *Mechanism and Machine Theory,* **39**(1), pp. 25–40.

[10] Arakelian, V., 2006, "Shaking moment cancellation of self-balanced slider–crank mechanical systems by means of optimum mass redistribution," *Mechanics Research Communications,* **33**(6), pp. 846–850.

[11] Van der Wijk, V., and Herder, J. L., 2009, "Dynamic balancing of Claver's Delta robot," In Computational Kinematics: Proceedings of the 5th International Workshop on Computational Kinematics, A. Kecskemethy and A. Müller, eds., Springer, pp. 315–322.

[12] Briot, S., Arakelian, V., Sauvestre, N., and Le Baron, J. P., 2010, "Shaking forces minimization of high-speed robots via an optimal motion planning," In ROMANSY 18 Robot Design, Dynamics and Control, Springer Vienna, pp. 307–314.

[13] Briot, S., Arakelian, V., and Le Baron, J.-P., 2012, "Shaking force minimization of high-speed robots via centre of mass acceleration control," *Mechanism and Machine Theory,* **57**, pp. 1–12.

[14] Geng, J., Arakelian, V., and Chablat, D., 2020, "Shaking force balancing of the delta robot," In International Design Engineering Technical Conferences and Computers and Information in Engineering Conference, Vol. 10: 44th Mechanisms and Robotics Conference (MR).

[15] Papadopoulos, E., and Abu-Abed, A., 1994, "Design and motion planning for a zero-reaction manipulator," In Proceedings of the IEEE International Conference on Robotics and Automation, p. 1554–1559.

[16] He, G., and Lu, Z., 2006, "Optimum motion planning of parallel redundant mechanisms with shaking force reduction," In The Proceedings of the Multiconference on "Computational Engineering in Systems Applications", Vol. 2, pp. 1132–1139.

[17] Ricard, R., and Gosselin, C. M., 2000, "On the de-

velopment of reactionless parallel manipulators," In International Design Engineering Technical Conferences and Computers and Information in Engineering Conference, Vol. 7A: 26th Biennial Mechanisms and Robotics Conference, pp. 493–502.

[18] Gosselin, C. M., Vollmer, F., Coté, G., and Wu, Y., 2004, "Synthesis and design of reactionless three-degree-of-freedom parallel mechanisms," *IEEE Transactions on Robotics and Automation,* **20**(2), pp. 191–199.

[19] Wu, Y., and Gosselin, C. M., 2004, "Synthesis of reactionless spatial 3-DoF and 6-DoF mechanisms without separate counter-rotations," *The International Journal of Robotics Research,* **23**(6), pp. 625–642.

[20] van der Wijk, V., and Herder, J. L., 2012, "Synthesis method for linkages with center of mass at invariant link point – pantograph based mechanisms," *Mechanism and Machine Theory,* **48**, pp. 15–28.

[21] van der Wijk, V., 2014, "Methodology for Analysis and Synthesis of Inherently Force and Moment-balanced Mechanisms - Theory and Applications," PhD thesis, University of Twente.

[22] Arakelian, V., and Briot, S., 2015, *Balancing of Linkages and Robot Manipulators - Advanced Methods with Illustrative Examples* Springer, Cham.

[23] Arakelian, V., 2017, "Inertia forces and moments balancing in robot manipulators: a review," *Advanced Robotics,* **31**(14), pp. 717–726.

[24] Feng, B., Morita, N., and Torii, T., 2002, "A new optimization method for dynamic design of planar linkage with clearances at joints-optimizing the mass distribution of links to reduce the change of joint forces," *Journal of Mechanical Design,* **124**(1), pp. 68–73.

[25] Chaudhary, K., and Chaudhary, H., 2015, "Optimal dynamic balancing and shape synthesis of links in planar mechanisms," *Mechanism and Machine Theory,* **93**, pp. 127–146.

[26] Bendsøe, M. P., and Sigmund, O., 2004, *Topology Optimization - Theory, Methods and Applications*, second ed. Springer-Verlag, Germany.

[27] Briot, S., and Goldsztejn, A., 2018, "Topology optimization of a reactionless four-bar linkage," In Computational Kinematics, S. Zeghloul, L. Romdhane, and M. A. Laribi, eds., Springer, Cham, pp. 413–421.

[28] Géradin, M., and Cardona, A., 2001, *Flexible Multibody Dynamics: A finite Element Approach* Wiley, England.

[29] Shabana, A. A., 2005, *Dynamics of Multibody Systems* Cambridge University Press, New York.

[30] Briot, S., and Goldsztejn, A., 2018, "Topology optimization of industrial robots: Application to a five-bar mechanism," *Mechanism and Machine Theory,* **120**, pp. 30 – 56.

[31] Chapman, C. D., and Jakiela, M. J., 1996, "Genetic algorithm-based structural topology design with compliance and topology simplification considerations," *Journal of Mechanical Design,* **118**(1), pp. 89–98.

[32] Li, G., Xu, F., Huang, X., and Sun, G., 2015, "Topology optimization of an automotive tailor-welded blank door," *Journal of Mechanical Design,* **137**(5).

[33] Deng, X., Wang, Y., Yan, J., Liu, T., and Wang, S., 2015, "Topology optimization of total femur structure: Application of parameterized level set method under geometric constraints," *Journal of Mechanical Design,* **138**(1).

[34] Liu, J., and To, A. C., 2019, "Computer-aided design-based topology optimization system with dynamic feature shape and modeling history evolution," *Journal of Mechanical Design,* **142**(7).

[35] Jiang, L., Gu, X. D., and Chen, S., 2020, "Generative design of bionic structures via concurrent multiscale topology optimization and conformal geometry method," *Journal of Mechanical Design,* **143**(1).

[36] Behzadi, M. M., and Ilieş, H. T., 2021, "GANTL: Toward practical and real-time topology optimization with conditional generative adversarial networks and transfer learning," *Journal of Mechanical Design,* **144**(2).

[37] Sigmund, O., 2007, "Morphology-based black and white filteres for topology optimization," *Structural and Multidisciplinary Optimization,* **33**, pp. 401–424.

[38] Qu, Z.-Q., 2004, *Model order reduction techniques with applications in finite element analysis* Springer-Verlag London, United Kingdom.

[39] Khalil, W., and Dombre, E., 2002, *Modeling, Identification and Control of Robot* Hermes Penton, London.

[40] Balay, S., Gropp, W. D., McInnes, L. C., and Smith, B. F., 1997, "Efficient management of parallelism in object oriented numerical software libraries," In Modern Software Tools in Scientific Computing, E. Arge, A. M. Bruaset, and H. P. Langtangen, eds., Birkhauser Press, pp. 163–202.

[41] Aage, N., Andreassen, E., and Lazarov, B. S., 2015, "Topology optimization using PETSc: An easy-to-use, fully parallel, open source topology optimization framework," *Structural and Multidisciplinary*

Optimization, **51**, pp. 565–572.

[42] Ahrens, J. P., Geveci, B., and Law, C. C. W., 2005, *The Visualization Handbook* Elsevier, ch. 36. ParaView: An End-User Tool for Large-Data Visualization, pp. 717–731.

[43] Bourdin, B., 2001, "Filters in topology optimization," *International Journal for Numerical Methods in Engineering,* **50**(9), pp. 2143–2158.

[44] Svanberg, K., 1987, "The method of moving asymptotes - a new method for structural optimization," *International Journal for Numerical Methods in Engineerging,* **24**(2), pp. 359–373.

[45] Brown, D., 2008, "Video modeling: Combining dynamic model simulations with traditional video analysis," In American Association of Physics Teachers Summer Meeting.